

Real-time Multilead Convolutional Neural Network for Myocardial Infarction Detection

Wenhan Liu, Mengxin Zhang, Yidan Zhang, Yuan Liao, Qijun Huang*, Sheng Chang, *Member, IEEE*,
Hao Wang, *Member, IEEE*, and Jin He, *Senior Member, IEEE*

Abstract—In this paper, a novel algorithm based on a Convolutional Neural Network (CNN) is proposed for Myocardial Infarction (MI) detection via multilead electrocardiogram (ECG). A beat segmentation algorithm utilizing multilead ECG is designed to obtain multilead beats, and Fuzzy Information Granulation (FIG) is adopted for preprocessing. Then the beats are input into our Multilead-CNN (ML-CNN), a novel model that includes sub 2-D convolutional layers and Lead Asymmetric Pooling (LAP) layers. As different leads represent various angles of the same heart, LAP can capture multiscale features of different leads, exploiting the individual characteristics of each lead. In addition, sub 2-D convolution can utilize the holistic characters of all the leads. It uses 1-D kernels shared among the different leads to generate local optimal features. These strategies make the ML-CNN suitable for multilead ECG processing. To evaluate our algorithm, actual ECG datasets from the PTB diagnostic database are used. The sensitivity of our algorithm is 95.40%, the specificity is 97.37%, and the accuracy is 96.00% in the experiments. Targeting lightweight mobile healthcare applications, real-time analyses are performed on both MATLAB and ARM Cortex-A9 platforms. The average processing times for each heartbeat are approximately 17.10 ms and 26.75 ms, respectively, which indicates that this method has good potential for mobile healthcare applications.

Index Terms—Convolutional Neural Network (CNN), electrocardiogram (ECG), sub 2-D convolution, Lead Asymmetric Pooling (LAP), Myocardial Infarction (MI), real-time application.

I. INTRODUCTION

MYOCARDIAL Infarction (MI), with a pathology of coronary artery atherosclerosis [1], is one of the most common Cardiovascular Diseases (CVD). Due to blockage of the coronary vessels and small branches, the blood supply to the myocardium is insufficient, causing the myocardial cells to experience phases of ischemia, injury and necrosis. MI can be categorized into various types based on the portion of myocardial necrosis, including anterior MI, inferior MI, posterior MI, and so on. MI is a severe threat to human health.

This work was supported by the National Natural Science Foundation of China (61574102 and 61404094), the Fundamental Research Fund for the Central Universities, Wuhan University (2042015kf0174 and 2042016kf0189), the Natural Science Foundation of Hubei Province, China (2014CFB694), and the Hubei Province Science & Technology Pillar Program (grant no 2015CFB536).

W. Liu, M. Zhang, Y. Liao, Y. Zhang, Q. Huang, S. Chang, H. Wang and J. He are with the School of Physics and Technology, Wuhan University, Wuhan 430072, China (e-mail: huangqj@whu.edu.cn).

According to data from the *American Heart Association* (AHA) [2], 750,000 Americans suffered from MI in 2013, with approximately 116,000 deaths. Thus, it is of great significance to investigate MI monitoring and detection. The electrocardiogram (ECG) has played an important role in the development of MI diagnosis methods for decades due to its efficiency, and it merits additional research [3].

The ECG is a bioelectrical signal generated by the heart muscle. It is one of the most reliable and effective non-invasive diagnostic tools for MI [4]. In addition, Cine Magnetic Resonance (CMR) and Multidetector Computed Tomography (MDCT) are also adopted to diagnose MI [5], [6] but more professional expertise and expensive medical equipment are required when compared with using ECG. The standard 12-lead ECG system is widely applied in medical institutions, and MI can be diagnosed based on typical features of ECG waveforms or morphologies in multiple leads [7], such as the ST-segment changes, the T-wave inversions and abnormal Q-waves. However, MI detection is a tedious and difficult procedure for cardiologists, especially in places outside of a hospital environment. Hence, automatic MI detection, which can be applied in multiple scenarios such as home and community applications, has generated research interest of researchers in diverse fields.

Several methods have been used for automatic MI detection via ECG. Because multiple leads can provide more useful information for the algorithm than a single to obtain higher accuracy [7], multilead ECG is usually used. Most of the studies were based on the conventional machine learning framework, which generally consists of feature extraction and classification. In the feature extraction stage, some studies adopted hand-crafted manual features associated with ECG waveforms, such as QRS-waves, ST-segment, and ST-T complex [8]-[11]. Global features were also used to represent the beats by applying Principal Component Analysis (PCA) [12], Wavelet Transform (WT) [12], [13], polynomial fitting [14], [15], Hidden Markov Models (HMM) [16] or other techniques. In the classification stage, feature vectors were input into various classifiers for MI detection. The most common classifiers were Neural Networks (NN) [8], [11], [12]-[14], [17], Support Vector Machines (SVM) [10], [12], [14], [16], [18], K-Nearest Neighbors (KNN) [14], [18], decision trees [10], [15], and Random Forests (RF) [14]. Although these methods showed good performance, they also

exhibited obvious drawbacks. Methods based on the morphology features largely depend on the accuracy and robustness of fiducial points detection algorithms, and only the QRS detection algorithms are sufficiently reliable [19]. In addition, techniques such as PCA, WT and polynomial fitting are computationally expensive to suit real-time applications [20].

Recently, the deep learning technique has received attention from both academia and industry. It has led to considerable progress in many domains [21] such as natural language processing, speech recognition, image processing, and healthcare monitoring [22], [23]. A Convolutional Neural Network (CNN) is a typical deep learning architecture that imitates the biological visual system. It consists of three types of layers: convolutional layers, pooling layers, and fully-connected layers. As a successful deep learning technique, CNN and its modified versions have excellent performance in image recognition [24], [25]. For example, LeNet-5 can recognize hand-written characters accurately (accuracy > 95%) in real time [26]. Some algorithms based on CNNs have been applied to ECG analysis. For instance, a real-time 1-D CNN was utilized for arrhythmia classification based on single-lead ECG data [27]. It achieved good performance and had low computational complexity. A cascaded CNN model was also used to detect abnormal heartbeats [28] and was shown to be sufficiently robust for real-world ECG analysis. Stanford Machine Learning Group, a famous machine learning group directed by Andrew Ng, recently proposed a CNN-based arrhythmia detection algorithm using single-lead ECG [29]. It achieved better performance than that of the cardiologists in their experiment. Thus, compared with the conventional methods for MI detection using multilead ECG, the CNN-based algorithm can be a better choice. However, only single-lead ECG was employed in prior research [27]-[29] and the methods were only analyzed using computers. Because multilead ECG represents synchronized information from various angles and distances of the same heart, it has a unique data form that is different from those of normal 1-D signals and 2-D images. Therefore, traditional CNNs should be modified for multilead ECG.

With the rapid development of the Internet and sensor technologies, a series of mobile ECG healthcare systems have been proposed. Gao *et al.* [30] designed a 7-lead ECG daily monitoring system that uses smartphones to detect CVDs. The system could function for up to 44 hours on battery power due to a low-power design. WE-CARE, another 7-lead mobile monitoring system, was also developed [31], [32]. It utilized the light-loading Manifold-based ECG-feature Purification (MEP) algorithm [32]. Fang *et al.* [33] and John *et al.* [34] presented 3-lead ECG monitoring systems based on a System-On-Chip (SOC), providing real-time analysis of the heart state. Shimmer, a small-size and lightweight ECG wearable platform developed by Intel's digital health group, can detect arrhythmia using 3-lead ECG in real time [35]. Mobile ECG healthcare systems are different from professional medical systems. Firstly, most mobile systems employ only a portion of the 12 standard leads because they must be portable

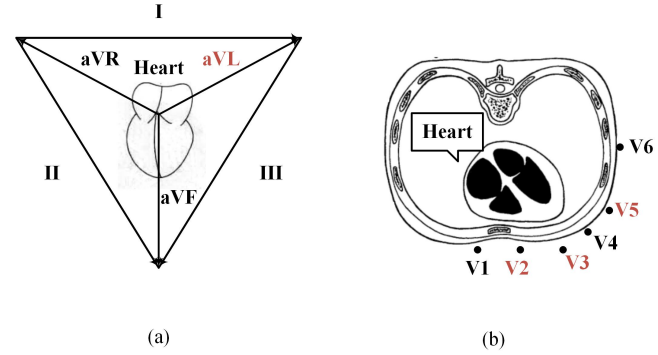


Fig. 1. Acquisition of cardiac electrical activity via 12-lead ECG. (a) 6 standard limb leads. (b) 6 precordial leads.

or wearable. Secondly, they are generally based on micro-embedded platforms including smartphones and SOC. Therefore, the algorithms applied in mobile ECG healthcare systems must be not only accurate but also of low complexity and real time. In fact, it is difficult for the existing systems to meet these requirements.

In this paper, a Multilead-CNN (ML-CNN) targeting mobile ECG healthcare system applications is proposed for the MI detection. Unlike algorithms based on a conventional machine learning framework, the ML-CNN is independent of hand-designed features due to its remarkable automatic feature learning ability. The significance of our paper lies in three main aspects:

1) In the preprocessing stage, a beat segmentation algorithm that can utilize multiple leads is presented. Fuzzy Information Granulation (FIG) is employed to preprocess the raw beat data to enhance the robustness of our algorithm.

2) To optimize the ML-CNN for multilead ECG processing, sub 2-D convolution and Lead Asymmetric Pooling (LAP) strategy are designed to utilize the intra-lead local changes and multiscale features in different leads. These methods allow for the ML-CNN to outperform the regular 2-D CNN and achieve good results.

3) The entire flow of the proposed algorithm, from beat segmentation to the final decision making in ML-CNN, is implemented using a real-time micro-embedded system. This indicates that the algorithm has a good potential to be used in mobile monitoring applications.

The remainder of this paper is organized as follows. Section II briefly introduces the ECG database used in this paper and describes some of the basic settings. The main content of our algorithm is presented in Section III, including the beat segmentation, FIG, and ML-CNN. The experimental results and discussion are presented in Section IV. Section V concludes the paper.

II. DATA SOURCE AND BASIC SETTINGS

In this study, the ECG data are obtained from the Physikalisch-Technische Bundesanstalt (PTB) diagnostic database [36]. This database is composed of 549 records from 290 individuals and is provided by the National Metrology Institute of Germany. The ECGs are collected from healthy volunteers and patients with different heart diseases by

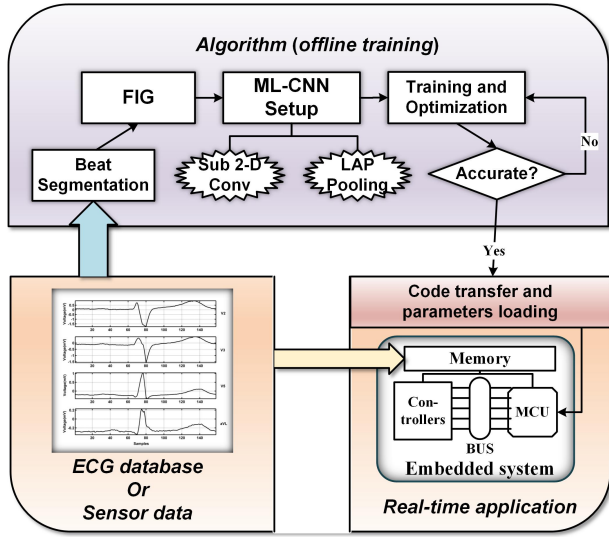


Fig. 2. Flowchart of the proposed algorithm.

TABLE I
NUMBER OF RECORDS IN DIFFERENT CLASSES

Class	Number of Records
GAMI (class 1)	167
HC (class 0)	80
Total	247

TABLE II
CORRESPONDING GAMI LEADS

Portion	Leads
Anterior	V3,V4
Septal	V1,V2
Lateral	I,aVL,V5,V6

Professor Michael Oeff, M.D., at the Department of Cardiology of the Benjamin Franklin University Clinic in Berlin, Germany. Each record contains 12 conventional leads (I, II, III, aVR, aVL, aVF, V1, V2, V3, V4, V5, and V6, as shown in Fig. 1) and 3 Frank leads (VX, VY, and VZ). The sampling rate is 1 kHz, with 16-bit resolution over a ± 16.384 mV range. According to the statistics, 368 records in the database are related to MI and 80 records are from 52 healthy subjects, which are termed Healthy Controls (HC). The remainder of the records are from subjects suffering from other CVDs such as heart failure and bundle branch block. The ECG records are typically of 2 minutes in duration, and all the signals last at least 30 s.

Different types of MI have distinctive morbidities. A considerable proportion of patients (greater than 50%) encounter Generalized Anterior MI (GAMI), including anterior MI, anteroseptal MI and anterolateral MI [1]. Therefore, in this paper, we concentrate on GAMI. The database provides 47 anterior MI, 77 anteroseptal MI, and 43 anterolateral MI records. There are $(47 + 77 + 43) = 167$ GAMI records from 60

subjects. The records used for automatic detection by ML-CNN are described in Table I.

Because our algorithm is intended for mobile monitoring applications rather than professional medical research, we choose relevant leads instead of using all 12 leads to maintain a low-complexity algorithm. Each lead corresponds to a section of the heart [37]. According to Table II, there are 8 leads related to GAMI [16]. Half of these leads are utilized in our algorithm, including V2, V3, V5 and aVL. They can detect all the 3 related categories. For the anterior wall, V3 is selected because it is the closest lead to the heart [38]. V2 has larger R waves than V1 [39], which means that V2 can easily be analyzed by the algorithm. Thus, V2 is employed to represent the septal wall. For the lateral wall, V5 is selected because it has the highest sensitivity in detecting myocardial ischemia [40]. A limb lead is used to reflect the lateral wall. To maintain consistency, aVL is chosen because it is a unipolar lead in addition to the precordial leads. Notably, aVL is more reasonable for diagnosing MI caused by Left Anterior Descending (LAD) coronary artery occlusion, especially extensive anterior MI [41]. Thus, the amount of data to be processed can be reduced and the algorithm can be more suitable for wearable and portable devices. Because the ECG signal frequency bandwidth is 0.05-100 Hz, each record is resampled to 250 Hz, which is sufficient to reflect the useful frequency components.

III. METHOD

The procedure for our algorithm includes preprocessing and ML-CNN analysis. In the preprocessing stage, heartbeats are detected and segmented from the ECG signal. Then, FIG is performed for each heartbeat. The ML-CNN is trained and optimized using data from the previous stage, providing a prediction for each multilead heartbeat. When the algorithm achieves the most accurate result under a specific parameter configuration, it is transplanted to the embedded system for real-time application. A flowchart of the proposed algorithm is shown in Fig. 2. The design of our algorithm is based on 4 attributes included in multilead ECG: *singularity*, *semi-qualitative description*, *integrity*, and *diversity*. Detailed explanations of these attributes and the principles of our algorithm follow.

A. Beat Segmentation and FIG

The heartbeat (or beat for short) is the basic unit of ECG, which can be characterized by successive waveforms including the P wave, QRS complex and T wave. From a mathematic perspective, the first attribute of multilead ECG can be described as:

Singularity: The QRS complex has characteristic steep slopes and sharp changes, which can be utilized in derivative-based operations [19].

Thus, a beat segmentation algorithm exploiting the *singularity* is designed to obtain multilead beats. Four or more leads can be utilized by the algorithm, and complex transforms such as wavelet transform and Hilbert transform are not involved in the operations. Hence, this algorithm is suitable for multilead ECG processing and is simple enough for embedded

platform implementation.

The first-order derivative is adopted to utilize the steep slope of the QRS complex. For each lead, it is given as:

$$y_i(n) = x_i(n+1) - x_i(n) \quad (1)$$

where $x_i(n)$ and $y_i(n)$ correspond to the raw signal and the differentiated signal of the i th lead, respectively. The first-order derivative can be treated as a high-pass filter [19], enhancing the QRS waves and alleviating the P waves and T waves. The differentiated signals from different leads are combined using the Mean Square (MS), which is formulated as:

$$s(n) = \frac{1}{Ld} \sum_{i=1}^{Ld} y_i^2(n) \quad (2)$$

where $s(n)$ is the new feature signal and Ld denotes the total number of leads, which is 4. The feature signal $s(n)$ exploits information from multiple leads. Fig. 3(a) shows an example of the raw multilead ECG and its feature signal.

As shown in Fig. 3(a), each multilead heartbeat corresponds to a sharp peak. To locate these peaks, a local maximum search is performed on the entire feature signal. Let j be the index of feature signal s ; for each $s(j)$, the criteria for local maximum can be set as:

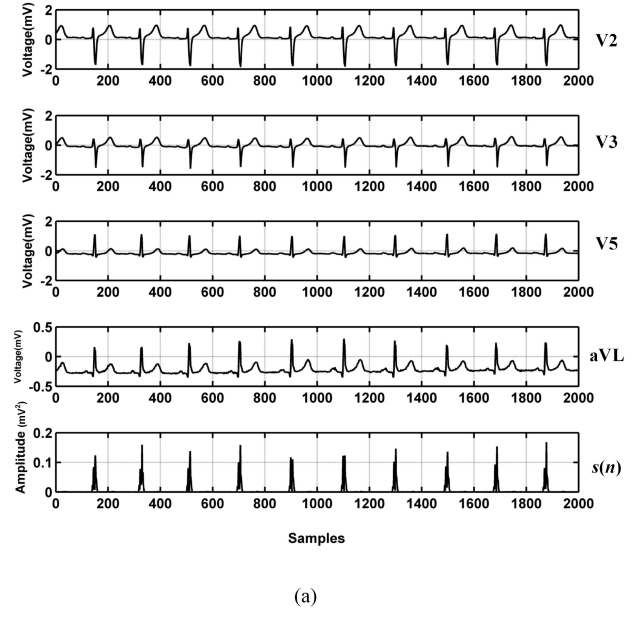
$$\begin{cases} s(j) - s(j-i) > 0 \\ \quad \& \quad, i=1,2,\dots,Lg \\ s(j) - s(j+i) > 0 \end{cases} \quad (3)$$

The two criteria in (3) ensure that $s(j)$ is the maximum of the local subsequence $[s(j-Lg), s(j-(Lg-1)), \dots, s(j), s(j+1), \dots, s(j+Lg)]$. Lg is an empirical parameter set to 10 here. An adaptive threshold strategy is used to verify all of the local maximums. It can determine candidates that represent the positions of the corresponding heartbeats. The adaptive mechanism can be described as:

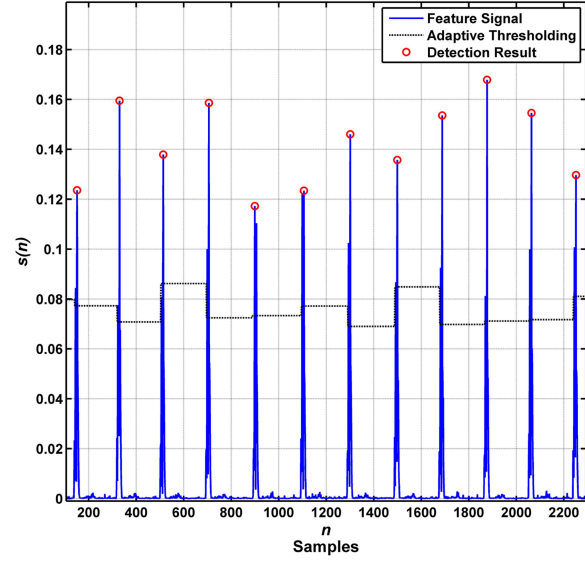
$$\theta = \begin{cases} 0.625 \cdot P(L), \theta \leq 0.625 \cdot \bar{P} \\ 0.5 \cdot P(L), \theta > 0.625 \cdot \bar{P} \end{cases} \quad (4)$$

where P is the sorted amplitudes of all peaks satisfying the aforementioned conditions, θ denotes the adaptive threshold, $P(L)$ is the last element of P , and \bar{P} is the average value of P . In addition, if two adjacent peaks that exceed the adaptive threshold are too close to each other (< 0.24 s or 60 sample points), the algorithm will select the peak whose amplitude is larger. Owing to the adaptive threshold, the peaks corresponding to the heartbeats are extracted and peaks caused by noise are discarded. Notably, the coefficients in (4) are empirical parameters and they are experimentally determined to ensure detection of the most beats. Fig. 3(b) shows an example of the adaptive threshold and detection results.

After peak detection, the locations of the detected peaks are



(a)



(b)

Fig. 3. An example of (a) the raw multilead ECG and its feature signal and (b) the adaptive threshold and detection results.

used as datum points to segment the heartbeats from each lead as follows:

$$b_{ij} = [x_i(I_j - N), x_i(I_j - N + 1), \dots, x_i(I_j), x_i(I_j + 1), \dots, x_i(I_j + N + 1)] \quad (5)$$

where b_{ij} refers to the j th beat in the i th lead, I_j is the index of the j th peak of the feature signal, and N is the parameter that determines the length of b_{ij} , which is set to 78 by trial and error. Hence, in (5), the length of b_{ij} is $((N + 1) + N + 1) = 158$.

Because human recognition with fuzzy conception is more robust and tolerant than the processing with accurate

computation, FIG based on fuzzy logic and information granulation is employed to process the beats. The second attribute of multilead ECG is utilized in FIG, which can be explained as:

Semi-qualitative: ECG data are a type of time series that can be described in a “semi-qualitative manner by pointing at specific regions” [42], so FIG is suitable for processing and interpreting it.

Considering the principle of simplicity, the FIG scheme called the W. Pedrycz method [43] is employed. A triangular membership function as shown in (6) is used to describe the fuzzy concept:

$$A(z, a, m, c) = \begin{cases} 0, z < a \\ \frac{z-a}{m-a}, a \leq z \leq m \\ 1 - \frac{z-m}{c-m}, m \leq z < c \\ 0, c \leq z \end{cases} \quad (6)$$

The purpose of FIG is to determine three parameters (6): a , m , and c . The W. Pedrycz method consists of the following 4 steps:

1) *Subsequence segmentation:* For a given sequence b_{ij} formulated as in (5), the k th subsequence of b_{ij} is obtained by:

$$b_{ij}^k = [x_i(I_j - N + k - 1), x_i(I_j - N + k), \dots, x_i(I_j - N + k + M - 2)] \quad (7)$$

where M denotes the length of b_{ij}^k .

2) *Determine m_{ij}^k (kernel of the fuzzy set):* First, the method rearranges b_{ij}^k in ascending order. Then, the median of b_{ij}^k is used as the kernel of the fuzzy set, i.e., $m_{ij}^k = \text{median}(b_{ij}^k)$.

3) *Determine a_{ij}^k (support lower bound of the fuzzy set):* Maximize a function with respect to a_{ij}^k , which is formulated as:

$$\arg \max Q(a_{ij}^k) = \frac{\sum_{x_i(n) \leq m_{ij}^k} A[x_i(n)]}{m_{ij}^k - a_{ij}^k} \quad (8)$$

where n refers to the index of the subsequence and a_{ij}^k runs through all elements of $x_i(n)$ that meet $x_i(n) \leq m_{ij}^k$. $A[\cdot]$ denotes the triangular membership function defined in (6).

4) *Determine c_{ij}^k (support upper bound of the fuzzy set):* Similar to step 3:

$$\arg \max Q(c_{ij}^k) = \frac{\sum_{x_i(n) > m_{ij}^k} A[x_i(n)]}{c_{ij}^k - m_{ij}^k} \quad (9)$$

where c_{ij}^k runs through all elements of $x_i(n)$ that meet $x_i(n) >$

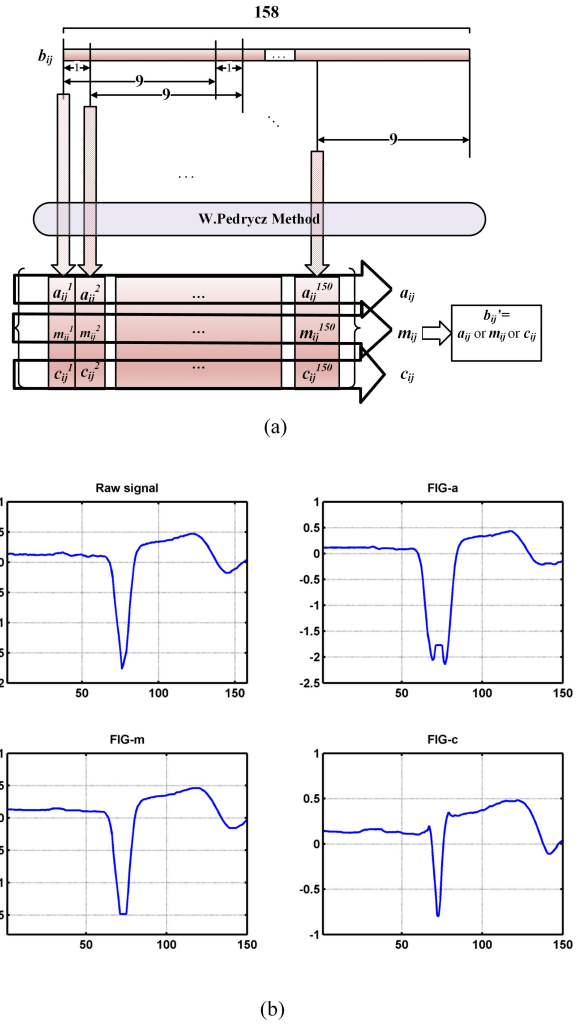


Fig. 4. (a) The FIG procedure on a single-lead beat. The numbers denote the sequence lengths. (b) A heartbeat and its approximations using FIG.

$$m_{ij}^k.$$

In the FIG procedure, the length of each subsequence (M) is set to 9 and two adjacent subsequences overlap each other at 8 points. Thus, the length of a beat is shortened by 8 points after FIG ($158 - 8 = 150$). The beats can be implied by a series of a , m , or c , as shown in (10):

$$b_{ij}' = \begin{cases} [a_{ij}^1, a_{ij}^2, \dots, a_{ij}^{150}]; \\ [m_{ij}^1, m_{ij}^2, \dots, m_{ij}^{150}]; \\ [c_{ij}^1, c_{ij}^2, \dots, c_{ij}^{150}]; \end{cases} \quad (10)$$

where b_{ij}' represents the single-lead beat after processing using the W. Pedrycz method. Fig. 4(a) illustrates the FIG procedure, and Fig. 4(b) shows a heartbeat and its approximations using the FIG method. Moreover, each multilead beat is generated by stacking its corresponding single-lead beats, as formulated in (11):

$$B_j = [b_{1j}', b_{2j}', b_{3j}', b_{4j}']^T \quad (11)$$

where B_j refers to the j th multilead beat in a record and $b_{1j}', b_{2j}', b_{3j}',$ and b_{4j}' ($i=1, 2, 3, 4$ in b_{ij}') denote beats described by sequences of $a, m,$ or c in leads V2, V3, V5, and aVL, respectively. In the aforementioned parameter configuration, the size of matrix B_j is 4×150 .

B. ML-CNN

CNN is a typical deep learning technique derived from the conventional Multi-Layer Perceptron (MLP). A typical CNN is composed of convolutional layers, pooling layers in the first few stages, and fully-connected layers (MLP) in subsequent stages. CNNs are generally trained using error backpropagation rules based on Feedforward Pass (FP) and Backpropagation Pass (BP) iterations. Each layer has its own feature maps, which refer to its inputs and outputs. The most important reason for the success of CNNs in image recognition is that **CNNs can efficiently capture local changes** [24]. However, in multilead ECG beats, only local changes in a single lead are meaningful for CNNs because only the intra-lead signal amplitudes are continuous and the inter-lead signal amplitudes are discontinuous.

Although multilead beats are treated as 2-D matrices in this study, they differ from standard 2-D data such as images in two unique attributes. Modifications of a CNN are based on the 2 attributes:

Integrity: Different leads reflect the status of the same heart. Thus, the intra-lead local changes in multilead ECG integrally determine the detection results. In the algorithm, they should be considered as a whole.

Diversity: Multilead ECG is acquired synchronously based on various angles and distances from the heart [38]. Thus, it is reasonable to conclude that multilead ECG reflects multiscale features of the heart.

However, conventional 2-D CNNs do not fit the aforementioned attributes. Meaningful intra-lead multilead ECG local changes cannot be captured in conventional 2-D convolutions, and normal pooling based on a single pooling factor cannot efficiently utilize the multiscale features. Considering the unique attributes of multilead ECG, ML-CNN for MI detection is proposed. The standard 2-D convolution and normal pooling in the conventional CNN are replaced with sub 2-D convolution and the LAP strategy, respectively. Moreover, the sub 2-D convolutional layers alternate with the LAP layers. The input of the ML-CNN is the 2-D multilead beat (B_j), given in (11).

As in conventional 2-D CNNs, training of the ML-CNN is based on reducing the error between the desired output and the actual output, which is given as:

$$E = \frac{1}{2} \sum_{k=1}^t (D_k - Y_k)^2 \quad (12)$$

where t is the number of categories and D_k and Y_k denote the desired output and the actual output, respectively. The actual output, Y_k , is determined by the ML-CNN and the input feature maps. The desired output, D_k , is determined by the label of the

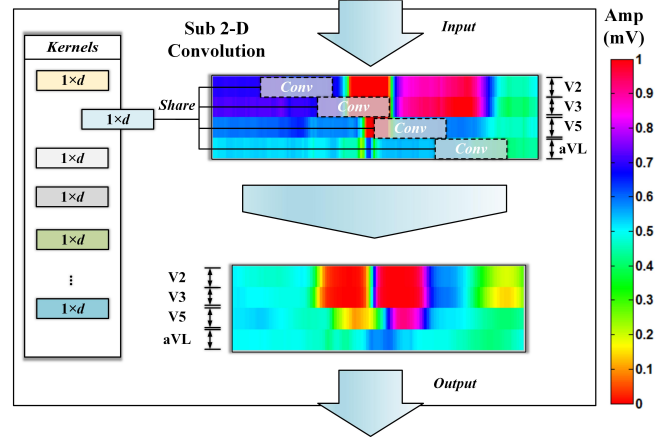


Fig. 5. An example of the sub 2-D convolution. The colors of the feature maps represent the variety of signal amplitudes.

corresponding input feature maps. The MLP in ML-CNN is the standard MLP used in many studies [21], [24], [44], so its training rules are not presented here.

1) Sub 2-D convolution

To maintain the *integrity* of the multilead ECG, sub 2-D convolution is designed to replace the standard 2-D convolution. When sub 2-D convolution is performed, **1-D horizontal kernels are utilized to detect the local changes**. Therefore, the detected local changes are all **intra-lead** and thus are meaningful for the ML-CNN. In the analysis above, a key issue is how to treat the intra-lead local features or changes from different leads as a whole. **The sub 2-D convolution shares its 1-D kernels among different leads**. Hence, the training algorithm can optimize the kernel parameters based on all the leads rather than a certain single lead. Compared with the scheme that uses specific kernels for each lead, the number of parameters in the sub 2-D convolutional layer is reduced, which can avoid overfitting to certain extent.

The inputs of convolutional layers are the previous layer's feature maps, and convolutions using multiple 1-D kernels shared among different leads are performed on the selected maps. An activation function is used to introduce non-linearity and generate the output feature maps. The FP procedure for the convolutional layers can be described as:

$$\begin{cases} u_j^l = \sum_i X_i^{l-1} * K_{ij}^l + b_j^l \\ X_j^l = f(u_j^l) \end{cases} \quad (13)$$

where X_j^l denotes the j th output feature map of layer l , $*$ denotes the sub 2-D convolution, K_{ij}^l is the 1-D kernel used to connect X_j^l with X_i^{l-1} , b_j^l is the bias corresponding to X_j^l , u_j^l is the linear combiner output, and $f(\cdot)$ represents the activation function; here, a sigmoid function is adopted. Fig. 5 illustrates the sub 2-D convolution on 2-D multilead ECG. Each output map of the sub 2-D convolution layers is obtained by the accumulation of all the output maps of the previous layers convolved with a certain kernel. Thus, the sub 2-D convolutional layers are fully connected with the previous layers.

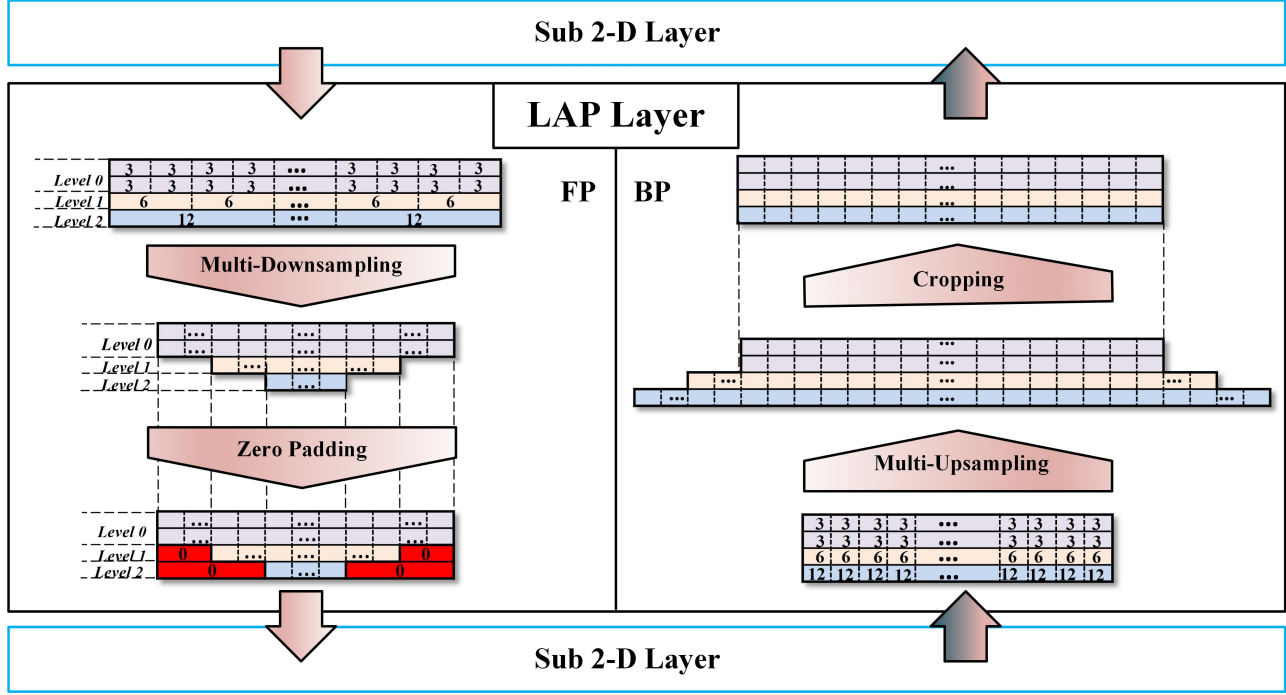


Fig. 6. An example of LAP. The grid squares denote feature maps in the FP stage or δ s in the BP stage. Positive numbers in the squares refer to downsampling or upsampling factors. ‘0’s in the FP should be padded to the feature maps. Apostrophes denote the omission of data samples.

In the BP procedure, a key parameter (δ_j^l) that denotes the derivative of the predicted error with respect to u_j^l is defined as:

$$\delta_j^l = \frac{\partial E}{\partial u_j^l} = \frac{\partial E}{\partial X_j^l} \frac{\partial X_j^l}{\partial u_j^l} \quad (14)$$

The derivative of the predicted error with respect to the feature map X_i^{l-1} can be obtained by:

$$\frac{\partial E}{\partial X_i^{l-1}} = \sum_j \frac{\partial E}{\partial u_j^l} \frac{\partial u_j^l}{\partial X_i^{l-1}} = \sum_j \delta_j^l \otimes \text{reverse}(K_{ij}^l) \quad (15)$$

where \otimes refers to the sub 2-D convolution with zero padding, which is termed the full convolution. Let K_s denote the size of K_{ij}^l . The algorithm will pad $(K_s - 1)$ zeros to the left and right boundary of δ_j^l before convolution. A function $\text{reverse}(\cdot)$ is used to reverse the 1-D kernels. After determining all the corresponding δ_j^l , the derivative of the predicted error with respect to the layer’s bias can be obtained by:

$$\frac{\partial E}{\partial b_j^l} = \sum_{u,v} (\delta_j^l)_{uv} \quad (16)$$

To compute the derivative with respect to a kernel, all of the derivatives connected with the kernel should be summed using a convolution operation:

$$\frac{\partial E}{\partial K_{ij}^l} = \delta_j^l * \text{rot180}(X_i^{l-1}) \quad (17)$$

where $\text{rot180}(\cdot)$ rotates a feature map 180 degrees. The updated rule of K_{ij}^l and b_j^l is similar to that of the weights and biases in MLP.

2) Lead Asymmetrical Pooling

In conventional 2-D CNNs, the pooling layers downsample their input feature maps by a certain factor (pooling factor) and produce a singular output for each non-overlapping sub-region. Notably, the normal pooling strategy cannot capture multiscale features in multilead ECG because a single pooling factor is used. According to several studies on image recognition [45]-[47], a multilevel pooling strategy can efficiently utilize multiscale features [45] and enhance the invariance of local features [46], [47], improving the accuracy of CNNs.

Thus, to manage the *diversity* of multilead ECG, the LAP strategy is designed to replace normal pooling. As an extension of this multilevel pooling strategy, LAP can utilize multiscale features by applying multiple pooling factors to multiple levels in accordance with the level division. The 4 leads are divided into 3 levels based on the electrode position namely *levels 0, 1* and *2*. V2 and V3 belong to the same level because their electrodes are close, and V5 and aVL belong to the other levels. Let p denote the basic pooling factor; thus, the actual pooling factor of each level can be given as:

$$P_L = p \cdot 2^L \quad (18)$$

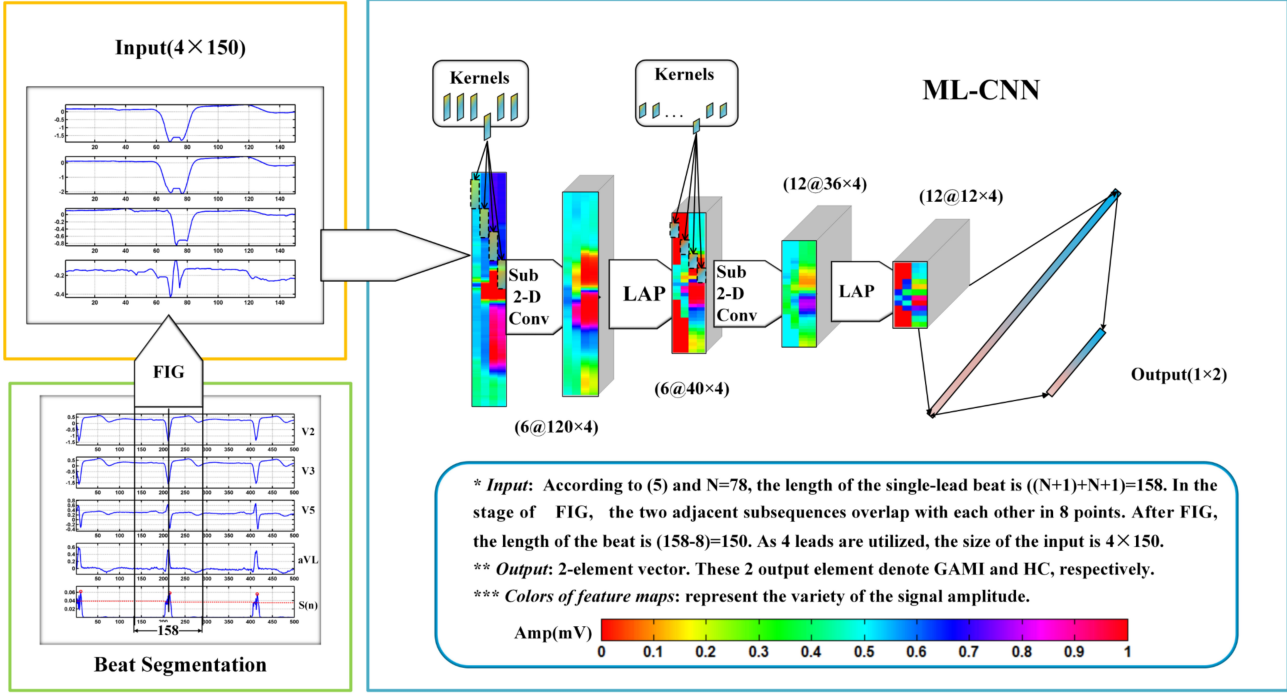


Fig. 7. An overview of the proposed method.

where $L = 0, 1$, or 2 corresponds to the 3 levels of the leads. For instance, if p is set to 3, V2 and V3 are *level 0*, V5 is *level 1*, aVL is *level 2*, and the pooling factors of the 4 leads will be 3, 3, 6 and 12, respectively. Lower levels indicate that smaller sub-regions are used to implement the pooling. Larger sub-regions are adopted to implement the pooling of higher levels, which are based on coarser information. Thus, the multiscale features contained in multilead ECG can be utilized simultaneously in our LAP strategy.

Due to application of multiple pooling factors, each level has a different signal length after pooling, which is unsuitable for further processing by the ML-CNN. Using the length of *level 0* as a reference, zeros are padded to the left and right boundaries of *levels 1* and *2*. Let n_0 denote the length of *level 0* and n_L denote the length of *level 1* or *2*; thus, the number of zeros padded can be given as:

$$\begin{cases} n_z^{left} = \left\lceil \frac{n_0 - n_L}{2} \right\rceil \\ n_z^{right} = n_0 - n_L - n_z^{left} \end{cases} \quad (19)$$

where n_z^{left} and n_z^{right} are the number of zeros padded to the left and right boundaries, respectively, and $\lceil \cdot \rceil$ denotes the ceiling operations. In addition, zero padding makes the features sparse, which can avoid overfitting to some extent.

Considering the principles of LAP, the equations of its FP can be described as:

$$X_j^l = \text{downM}(X_j^{l-1}) \quad (20)$$

where $\text{downM}(\cdot)$ denotes the multilevel downsampling with zero padding to compute the average values of sub-regions. Fig. 6 shows an example of the FP stage. Furthermore, the LAP layers subsample all the output maps of the previous sub 2-D layers by applying multiple pooling factors.

However, the BP stage of LAP has issues with inconsistent signal lengths because upsampling, the inverse operation of downsampling, is based on multiple pooling factors. In contrast with the zero padding in the FP stage, the feature maps are fitted to the expected size via cropping in the BP stage. Using the length of *level 0* as a reference, the number of data points cropped from the boundaries of *level 1* or *2* is given as:

$$\begin{cases} n_c^{left} = \left\lceil \frac{n_L - n_0}{2} \right\rceil \\ n_c^{right} = n_L - n_0 - n_c^{left} \end{cases} \quad (21)$$

where n_c^{left} and n_c^{right} are the number of data points cropped from the left and right boundaries, respectively. Compared with (14), the corresponding δ of a sub 2-D convolutional layer can be obtained more easily using:

$$\delta_j^l = \text{upM}\left(\frac{\partial E}{\partial X_j^{l+1}}\right) \circ f'(u_j^l) \quad (22)$$

where $\text{upM}(\cdot)$ denotes multilevel upsampling with cropping. The BP stage corresponding to the aforementioned FP stage is also shown in Fig. 6.

In summary, ML-CNN negates hand-designed features. It

TABLE III
PERFORMANCE OF ML-CNN UNDER DIFFERENT PARAMETER CONFIGURATIONS

FIG Parameter (<i>a/m/c</i>)	LAP Level Setting [V2,V3,V5,aVL]	SE (%)	SP (%)	Acc (%)
<i>a</i>	[0,0,1,2]	93.10	97.37	94.40
	[0,0,2,1]	91.95	94.73	92.80
	[1,1,0,2]	95.40	97.37	96.00
	[1,1,2,0]	89.66	86.84	88.80
	[2,2,0,1]	96.55	89.47	94.40
	[2,2,1,0]	95.40	84.21	92.00
<i>m</i>	[0,0,1,2]	87.35	94.73	89.60
	[0,0,2,1]	87.35	97.37	90.40
	[1,1,0,2]	90.80	89.47	90.40
	[1,1,2,0]	91.95	89.47	91.20
	[2,2,0,1]	94.25	92.10	93.60
	[2,2,1,0]	91.95	86.84	90.40
<i>c</i>	[0,0,1,2]	91.95	89.47	91.20
	[0,0,2,1]	89.66	86.84	88.80
	[1,1,0,2]	91.95	92.10	92.00
	[1,1,2,0]	90.80	84.21	88.80
	[2,2,0,1]	94.25	92.10	93.60
	[2,2,1,0]	91.95	92.10	92.00

combines feature extraction and classification in a single entity and is more reliable than the conventional framework. Moreover, ML-CNN functions by applying sub 2-D convolution and the LAP strategy to utilize specific attributes of 2-D multilead ECG. Overall, ML-CNN is designed to utilize the advantages of CNN and the unique attributes of 2-D multilead ECG to overcome the problems of conventional 2-D CNNs.

IV. EXPERIMENTAL RESULTS AND DISCUSSION

The performance of the ML-CNN in GAMI detection was evaluated based on the ECG records described in Section II. A real-time analysis was applied to test the practicability of the system. The experiments were based on an ML-CNN with two sub 2-D convolutional layers, two LAP layers and two MLP layers. For the two sub 2-D convolutional layers, the kernel sizes were set to 31 and 5 and the numbers of kernels were set to 6 and 12. The basic pooling factors in both LAP layers were set to 3. Thus, the numbers of MLP's input and output elements were 576 and 2, respectively, while no hidden layer was set in the MLP.

For the dataset partition, multilead beats segmented from 122 records constituted the training dataset. Those segmented from the remaining 125 records were used as the testing dataset. Although there were multiple recordings per patient, there were no patient overlaps between the training and testing sets. Each diagnostic result corresponds to a record rather than a multilead beat. If more than half of the beats were classified as GAMI, then the record was diagnosed as GAMI; otherwise, it was classified as HC. The experimental data comprised 34769 multilead beats, which consisted of 139076 single-lead beats and 17160 multilead beats used to train the algorithm. According to the empirical formula for the relationship between the training sample size and the model generalization [48], it is sufficient to obtain a good generalization (>90%). Moreover, stochastic gradient descent (SGD) [24] was adopted

TABLE IV
PERFORMANCE IMPROVEMENTS OF SUB 2-D CONVOLUTION AND LAP STRATEGY

FIG Parameter (<i>a/m/c</i>)	Algorithm	SE (%)	SP (%)	Acc (%)
<i>a</i>	1	95.40	86.84	91.20
	1+2	93.10	94.73	93.60
	1+2+3	95.40	97.37	96.00
<i>m</i>	1	90.80	89.47	90.40
	1+2	91.95	94.73	92.00
	1+2+3	94.25	92.10	93.60
<i>c</i>	1	91.95	84.21	89.60
	1+2	89.66	94.73	91.20
	1+2+3	94.25	92.10	93.60

*1: Regular 2-D CNN. 1+2: CNN with sub 2-D convolutions.
1+2+3: CNN with sub 2-D convolutions and LAP (ML-CNN)

in the training procedure. The batch size was set to 65, the learning rate was set to 0.17, and the maximum number of training iterations was set to 30. Fig. 7 shows the framework of the proposed method.

A. Diagnostic Performance Evaluation

The experiments in this section were based on three series of FIG parameters: *a*, *m*, and *c*. According to the principles of FIG, each parameter *a* represents the support lower bound of a fuzzy set. Thus, it can emphasize abnormal Q-waves and T-wave inversions in the MI records. Similarly, the parameter *c* can highlight the ST-segment elevations as it denotes the support upper bound. The procedure of determining parameter *m* is similar to well-known median filtering because the *m* of a subsequence is its median.

Based on the principles of LAP, level setting for a certain multilead beat can be divided into 6 ($A_3^3 = 3! = 6$) categories. Moreover, each beat can be implied by 3 FIG parameters (*a*, *m*, and *c*). Hence, there are 18 (6×3) parameter configurations for the performance evaluation, which is measured using the sensitivity (SE), specificity (SP) and accuracy (Acc). Let *TP* and *TN* denote the correctly detected MI and HC records, respectively, and *FP* and *FN* denote the incorrectly detected MI and HC records, respectively, by the ML-CNN. The three criteria can be defined as:

$$SE = \frac{TP}{TP + FN} \quad (23)$$

$$SP = \frac{TN}{TN + FP} \quad (24)$$

$$Acc = \frac{TP + TN}{TP + FN + FP + TN} \quad (25)$$

Table III summarizes the results under different parameter configurations. From a medical perspective, the appearance of pathological Q-waves is more reasonable for MI detection than the ST-segment changes [7]. Hence, the parameter *a*, which can emphasize these Q-waves through FIG, can lead to a better

TABLE V
THE 5-FOLD CROSS-VALIDATION RESULTS UNDER DIFFERENT PARAMETER CONFIGURATIONS

FIG Parameter ($a/m/c$)	LAP Level Setting [V2,V3,V5,aVL]	Average SE (%)	Average SP (%)	Average Acc (%)
<i>a</i>	[0,0,1,2]	94.68	91.27	93.53
	[0,0,2,1]	90.79	91.26	91.14
	[1,1,0,2]	95.43	93.21	94.76
	[1,1,2,0]	88.76	84.87	86.82
	[2,2,0,1]	92.75	90.17	92.24
	[2,2,1,0]	94.32	90.49	92.71
<i>m</i>	[0,0,1,2]	92.15	90.44	91.92
	[0,0,2,1]	93.11	91.38	91.94
	[1,1,0,2]	92.74	92.07	92.61
	[1,1,2,0]	91.67	86.02	88.62
	[2,2,0,1]	92.22	94.98	92.68
	[2,2,1,0]	92.69	82.35	88.98
<i>c</i>	[0,0,1,2]	90.01	94.35	92.22
	[0,0,2,1]	92.31	89.33	91.64
	[1,1,0,2]	91.51	93.76	92.33
	[1,1,2,0]	94.10	77.22	88.69
	[2,2,0,1]	92.79	94.50	92.93
	[2,2,1,0]	94.50	85.93	91.35

TABLE VI
PERFORMANCE COMPARISON OF THE PROPOSED METHOD AND OTHER METHODS

Method	SE (%)	SP (%)	Acc (%)
Reddy <i>et al.</i> [11]	79.00	97.00	N/A
Lu <i>et al.</i> [17]	89.40	95.00	N/A
Correa <i>et al.</i> [9]	93.90	93.44	93.73
Sun <i>et al.</i> [14]	91.00	85.00	N/A
Bhaskar <i>et al.</i> [12]	N/A	N/A	91.07
Sharma <i>et al.</i> [18]	93.00	99.00	96.00
Liu <i>et al.</i> [15]	N/A	N/A	94.40
Proposed	95.40	97.37	96.00

result. Moreover, V5 is proven to be the most sensitive lead in the diagnosis of myocardial ischemic disease [40], and V2 and V3 can reflect detailed information about the anterior and septal walls of the heart. In principle, these 3 precordial leads should be set to lower levels. In addition, aVL is a limb lead that conveys the general state of a heart. It contains coarser features and should be set to higher levels. This inference is in line with the experimental results. The sensitivity of the ML-CNN was 95.40%, the specificity was 97.37%, and the accuracy was 96.00% when the FIG parameter *a* was used and V2, V3, V5, and aVL were set to *level 1*, *level 1*, *level 0* and *level 2*, respectively.

Furthermore, additional experiments were conducted to demonstrate how the sub 2-D and LAP strategy improves the performance of the algorithm. The performance of algorithms with the optimum parameter settings is shown in Table IV, given a CNN model with regular 2-D convolutions using 2-D kernels ($2 \times d$) and normal pooling strategies as *algorithm 1*, CNN with the sub 2-D convolution as *algorithm 1+2*, CNN with the sub 2-D convolution and the LAP as *algorithm 1+2+3*. The sub 2-D convolution and LAP strategy can improve the performance of the model. Five-fold cross validation was used

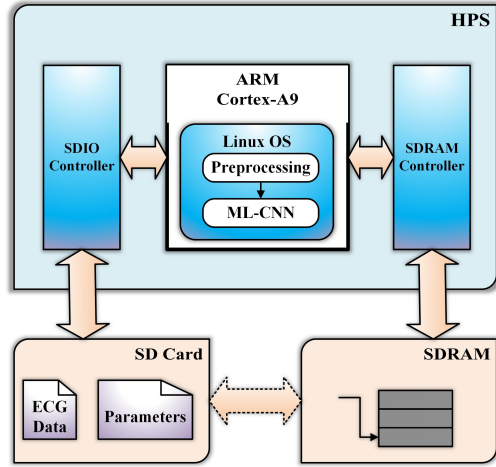


Fig. 8. The framework of the embedded system; hollow arrows with a solid line represent direct data exchanges, and those with dotted lines denote indirect data exchanges.

to further verify the reliability of the proposed method. The results are shown in Table V, including the average SE, SP and Acc for the folds. There was no patient overlap among the folds. Again, the best parameter configuration was (a, [1, 1, 0, 2]). The other configurations achieved similar performance as in the first-stage validation, which demonstrated that the algorithm is sufficiently stable.

In addition, our algorithm was compared with several methods reported in other studies, as shown in Table VI. Notably, our method has state-of-the-art performance. Due to the excellent feature learning ability of ML-CNN, no hand-designed features are utilized in our method. Sub 2-D convolution and the LAP strategy make the ML-CNN more suitable for multilead ECG analysis, which is the main reason for the good results.

B. Real-Time Analysis

To evaluate the real-time performance, our algorithm was implemented on a Windows PC and a micro-embedded platform. The algorithm was performed on a desktop computer with an Intel Core i7-3770(@ 3.4 GHz) CPU and 12GB RAM using MATLAB R2011a in 64-bit. Based on the testing dataset, the computation time required to perform the algorithm for 40-beat segments (20 s ~ 40 s) was measured. It took an average of 0.684 s for the algorithm to diagnose using a ML-CNN that was trained in the MATLAB environment. The processing of each beat can generally be completed in 17.10 ms (0.684/40 s), and the running time is proportional to the number of heartbeats.

For the embedded platform, ARM was employed in the real-time experiments. It is the most widely used embedded framework in real-world applications. The proposed algorithm was implemented on the Terasic DE1-SoC platform with an ARM Cortex-A9 processor (@ 925 MHz) and 1GB RAM using C code on a Linux operation system. All of the data were stored on an SD card. Considering the weak computational capacity of the ARM processor, the ML-CNN model that trained offline in MATLAB was transplanted to the system without extra

training. The model was deployed in the system as parameter files and C functions. Based on the Hardware Process System (HPS) framework shown in Fig. 8, the ARM processor can exchange data with the SD card and SDRAM through the SDIO and the SDRAM controllers, respectively. The resulting data were also exported to the SD card. For an ECG segment containing 40 heartbeats (20 s ~ 40 s), this embedded system took an average of 1.07 s to detect under the same precondition and parameter settings. The average time spent processing each beat was approximately 26.75 ms (1.07/40 s). Thus, the computational cost obtained was significantly less than the beat segment used [23], which demonstrated that the algorithm can satisfy real-time constraints. Furthermore, the experiments performed on ARM demonstrated that our algorithms can be efficiently applied to lightweight mobile healthcare systems.

V. CONCLUSION

In this study, a novel algorithm for MI detection using multilead ECG is proposed. Different from the conventional machine learning framework consisting of feature extraction and classification, our ML-CNN is capable of simultaneously learning features automatically and classifying the samples. Due to the sub 2-D convolution and LAP strategy, the ML-CNN is more suitable for multilead ECG analysis than conventional 2-D CNNs. The results show that it has a sensitivity of 95.40%, specificity of 97.37%, and accuracy of 96.00% for MI detection, comparable to methods with complex hand-designed features. Our algorithm's running times are sufficiently brief on both PC and ARM embedded platforms, which demonstrates that it can be applied in real-time systems. The implementation on ARM indicates the possibility of applications in mobile systems such as wearable or portable devices.

Although the proposed method has many advantages, there is room for further improvement. The algorithm contains numerous parameters; thus, tuning is required to obtain better results. For real-world applications, a complete hardware framework, including the front acquisition circuit, embedded platform and user interface, is essential. In the future, we will establish and apply a lightweight wearable or portable system based on our algorithm.

REFERENCES

- [1] V. Kumar, A. K. Abbas, N. Fausto, "The Heart," in *Robbins and Cotran Pathologic Basis of Disease*, 7th ed. Philadelphia: Elsevier Saunders, 2005, ch.12, pp. 555–618.
- [2] D. Mozaffarian, E.J.Benjamin *et al.*, "Executive Summary: Heart Disease and Stroke Statistics-2016 Update: A Report From the American Heart Association," *Circulation*, vol.133, no.4, pp. 447–454, 2016.
- [3] G. D. Clifford, F. Azuaje, and P. McSharry, *Advanced Methods and Tools for ECG Data Analysis*. Boston, MA: Artech House, 2006.
- [4] W. J. Tompkins, *Biomedical Digital Signal Processing*. Upper Saddle River, NJ, USA: Prentice-Hall, 1993.
- [5] A. Suinesiaputra *et al.*, "Statistical shape modeling of the left ventricle: myocardial infarct classification challenge," *IEEE J. Biomed. Health Informat.*, vol.PP, no.99, pp.1-1.Jan. 2017.
- [6] A. Mukhopadhyay, Z. Qian, S. Bhandarkar, T. Liu, S. Voros and S. Rienhart, "Morphological Analysis of the Left Ventricular Endocardial Surface Using a Bag-of-Features Descriptor," *IEEE J. Biomed. Health Informat.*, vol.19, no.4, pp.1483-1493, Sep. 2014
- [7] K. Thygesen *et al.*, "Third universal definition of myocardial infarction," *Circulation*, vol. 126, no. 16, pp. 2020–2035, 2012.
- [8] P. Bozzola, G. Bortolan, C. Combi, F. Pinciroli, and C. Brohet, "A hybrid neuro-fuzzy system for ECG classification of myocardial infarction," in *Proc. Comput. Cardiol.*, 1996, pp. 241–244.
- [9] R. Correa, P.D. Arini, L.S. Correa *et al.*, "New VCG and ECG Indexes for Early Identification of Acute Myocardial Infarction Patients," in *Proc. IFMBE*, 2015, pp.369–372.
- [10] D. Cao, D. Lin and Y. Lv, "ECG codebook model for Myocardial Infarction detection," in *Proc.10th Int. Conf. Nat. Comput.*, 2014, pp. 797-801.
- [11] M. R. S. Reddy *et al.*, "Neural network versus electrocardiographer and conventional computer criteria in diagnosing anterior infarct from the ECG," in *Proc. Comput. Cardiol.*, Oct. 1992, pp. 667–670.
- [12] N.A.Bhaskar, "Performance analysis of support vector machine and neural networks in detection of myocardial infarction," *Proc. Comput. Sci.*, vol.46, pp.20-30, 2015.
- [13] F.M.Al-Naima, A.H.Ali, S.S.Mahdi, "Data acquisition for myocardial infarction classification based on wavelets and neural networks," in *the 5th Int Multi-Conf. of IEEE Sys. Sig. and Devices*, Amman, pp.1-6, 2008
- [14] L. Sun *et al.*, "ECG analysis using multiple instance learning for myocardial infarction detection," *IEEE Trans. Biomed. Eng.*, vol. 59, no. 12, pp. 3348–3356, Dec. 2012.
- [15] B.Liu, J.Liu *et al.*, "A novel electrocardiogram parameterization algorithm and its application in myocardial infarction detection," *Comput. Biol. Med.*, vol.61, pp.178-184, Jun. 2015.
- [16] P.-C. Chang, J.-J. Lin, J.-C. Hsieh, and J. Weng, "Myocardial infarction classification using multi-lead ECG using hidden Markov models and Gaussian mixture models," *Appl. Soft Comput.*, vol. 12, no. 10, pp. 3165–3175, 2012.
- [17] H. L. Lu *et al.*, "An automated ECG classification system based on a neuro-fuzzy system," in *Proc. Comput. Cardiol.*, 2000, pp. 387–390.
- [18] L. N. Sharma, R. K. Tripathy and S. Dandapat, "Multiscale Energy and Eigenspace Approach to Detection and Localization of Myocardial Infarction," *IEEE Trans. Biomed. Eng.*, vol. 62, no. 7, pp. 1827–1837, Jul. 2015.
- [19] B. U. Köhler, C. Hennig, and R. Orglmeister, "The principles of software QRS detection," *IEEE Eng. Med. Biol.*, vol. 21, no. 1, pp. 42–57, Jan.-Feb. 2002.
- [20] D. Estrin *et al.*, "Embedded, Everywhere: A Research Agenda for Networked Systems of Embedded Computers," Nat'l Research Council Report, 2001.
- [21] J. Schmidhuber, "Deep learning in neural networks: An overview," *Neural Netw.*, vol. 61, pp. 85–117, 2015.
- [22] D. Ravi, C. Wong, B. Lo, *et al.*, "Deep Learning for Health Informatics," *IEEE J. Biomed. Health Informat.*, vol. 21, no. 1, pp. 4–21, Jan. 2017.
- [23] D. Ravi, C. Wong, B. Lo, *et al.*, "A Deep Learning Approach to on-Node Sensor Data Analytics for Mobile or Wearable Devices," *IEEE J. Biomed. Health Informat.*, vol. 21, no. 1, pp. 56–64, Jan. 2017.
- [24] Y. LeCun, Y. Bengio, and G. Hinton, "Deep learning," *Nature*, vol. 521, pp. 436–444, May 2015.
- [25] A. Krizhevsky *et al.*, "Imagenet classification with deep convolutional neural networks," in *Proc. Adv. Neural Inf. Process. Syst. Conf.*, 2012, pp.1106–1114.
- [26] Y. LeCun, L. Bottou, Y. Bengio, and P. Haffner, "Gradient-based learning applied to document recognition," *Proc. IEEE*, vol. 86, no. 11, pp. 2278–2324, Nov. 1998.
- [27] S. Kiranyaz, T. Ince, and M. Gabbouj, "Real-time patient-specific ECG classification by 1D convolutional neural networks," *IEEE Trans. Biomed. Eng.*, vol. 63, no. 3, pp. 664–675, Mar. 2016.
- [28] W. Yin, X. Yang, L. Zhang, *et al.* ECG Monitoring System Integrated With IR-UWB Radar Based on CNN. *IEEE Access*, vol. 4, pp. 6344-6351, Oct. 2016.
- [29] P. Rajpurkar, A.Y.Hannun, M. Haghpanahi, *et al.* "Cardiologist-Level Arrhythmia Detection with Convolutional Neural Networks." in *arXiv preprint arXiv:1707.01836*, 2017.
- [30] H. Gao, X. Duan, X. Guo, A. Huang, and B. Jiao, "Design and tests of a smartphones-based multi-lead ECG monitoring system," in *Proc. IEEE 35th Annu. Int. Conf. Eng. Med. Biol. Soc.*, Jul. 3–7, 2013, pp. 2267–2270.
- [31] A. Huang *et al.*, "We-care: An intelligent mobile telecardiology system to enable mhealth applications," *IEEE J. Biomed. Health Informat.*, vol. 18, no. 2, pp. 693–702, Mar. 2014.
- [32] A. Huang *et al.*, "System light-loading technology for mhealth: Manifold learning-based medical data cleansing and clinical trials in

- we-careproject," *IEEE J. Biomed. Health Informat.*, vol. 18, no. 5, pp. 1581–1589, Sep. 2014.
- [33] W.-C. Fang, H.-C. Huang, and S.-Y. Tseng, "Design of heart rate variability processor for portable 3-lead ECG monitoring system-on-chip," *Expert Syst. Appl.*, vol. 40, no. 5, pp. 1491-1504, Apr.2013.
- [34] D. John, Z. Xiaoyang, C. Heng, and L. Yong, "A 3-lead ECG-on-chip with QRS detection & lossless compression for wireless sensors," *IEEE Trans. Circuits Syst. II, Exp. Briefs*, 2016, doi: 10.1109/TCSII.2016.2613564
- [35] T.-B. Nguyen, W. Lou, T. Caelli, S. Venkatesh, and D. Phung, "Individualized arrhythmia detection with ECG signals from wearable devices," in *Proc. 2014 IEEE Int. Conf. Data Sci. Adv. Anal.*, 2014, pp. 570-576.
- [36] M. Oeff *et al.* (2012). "The PTB diagnostic ECG database," Nat. Metrol. Inst.Germany.[Online].Available:<http://www.physionet.org/physiobank/database/ptbdb>
- [37] I.Jekova *et al.*, "Inter-lead correlation analysis for automated detection of cable reversals in 12/16-lead ECG," *Comput. Meth. Prog. Bio.*, vol.134, pp.31-41, Oct. 2016.
- [38] J. Yu, Z. Wang, C. Yang, et al., "Comparison of Electrocardiographic Criteria for Diagnosis of Left Ventricular Hypertrophy," *Chin. Circ. J.*, vol.19, no.1, pp.28-30, Feb.2004.
- [39] A. L. Goldberger, *Clinical Electrocardiography: A Simplified Approach*. New York, NY, USA: Elsevier Health Sciences, 2012.
- [40] R. J. Gibbons. "ACC/AHA Guidelines for Ambulatory Electrocardiography," *J. Am. Coll. Cardiol.*, vol.34, no.3, pp.912-945, Sep. 1999.
- [41] B. Surawicz and T. K. Knilans, *Chou's Electrocardiography in Clinical Practice*. Philadelphia, PA: Saunders Elsevier, 2008
- [42] W. Pedrycz, *Granular Computing Analysis and Design of Intelligent Systems*. Boca Raton, FL, USA: CRC Press, 2013
- [43] W. Pedrycz, *Knowledge-Based Clustering: From Data to Information Granules*. Hoboken, NJ: Wiley, 2005.
- [44] D. Svozil, V. Kvasnicka, and J. Pospichal, "Introduction to multi-layer feed-forward neural networks," *Chemomet. Intell. Lab. Syst.*, vol. 39, no. 1, pp. 43–62, Nov. 1997
- [45] Y. Gong, L. Wang, R. Guo, and S. Lazebnik, "Multi-scale orderless pooling of deep convolutional activation features," in *Proc. 13th Eur. Conf. Comput. Vis.*, 2014, pp. 392–407.
- [46] S. Lazebnik, C. Schmid, and J. Ponce, "Beyond bags of features: Spatial pyramid matching for recognizing natural scene categories," in *Proc. IEEE Conf. Comput. Vis. Pattern Recognit.*, 2006, pp. 2169–2178.
- [47] K. He, X. Zhang, S. Ren, and J. Sun, "Spatial pyramid pooling in deep convolutional networks for visual recognition," *IEEE Trans. Pattern Anal. Mach. Intell.*, vol. 37, no. 9, pp. 1904–1916, Sep. 2015.
- [48] S. Haykin, *Neural Networks and Learning Machines*, 3rd ed. Cambridge, MA: Prentice-Hall, 2008